PASJ: Publ. Astron. Soc. Japan **48**, 557–564 (1996)

Evolution of the UV Background: The Effect of Radiative Cooling Photons from Collapsing Objects

Yuichiro INAGAKI and Shin SASAKI*
Department of Physics, School of Science, The University of Tokyo, Bunkyo-ku, Tokyo 113

(Received 1995 October 30; accepted 1996 May 7)

Abstract

We discuss the evolutions of the intensity and spectrum of the UV background radiation (UVB) in flat and open cold dark-matter universes. We consider two kinds of UV sources: one is QSOs, the other is collapsing objects, which liberate their binding energy radiatively. In the latter sources, we include the line emission corresponding to collisional excitation cooling of He II as well as free-free emission. We find that UV photons emitted from collapsing objects contribute to UVB as much as those from QSOs, and that the UVB spectrum becomes softer than that in the case in which only QSOs are taken into account. We also calculate the Gunn-Peterson optical depths assuming the ionization equilibrium, and compare them with observations.

Key words: Cosmic UV background — Cosmology — Galaxies : intergalactic medium — Lyα clouds — Quasars

1. Introduction

Recent observations of the Gunn-Peterson (GP) effects (Gunn, Peterson 1965; Jenkins, Ostriker 1991; Giallongo et al. 1992; Giallongo et al. 1994) and proximity effects (e.g., Bajtlik et al. 1988) indicate that there exists an intense metagalactic UV background (UVB) at high redshifts. Although QSOs have been the most popular candidate sources of UVB, it is still unclear whether or not they can provide a sufficient number of UV photons to be consistent with the observations (Bechtold et al. 1987; Shapiro, Giroux 1987; Meiksin, Madau 1993). Many authors have studied various models for the source of UVB, including young galaxies (Miralda-Escudé, Ostriker 1990; Fukugita, Kawasaki 1994), decaying dark-matter particles (e.g., Overduin et al. 1993), and the radiative cooling of gravitationally collapsing objects (Sasaki et al. 1993; Sasaki, Takahara 1994). However, there has been no consensus about the source of UVB. Recently, Jakobsen et al. (1994) have reported that they detected He II absorption in the spectrum of the quasar Q0302−003 at $z \simeq 3.286$. Although we cannot distinguish between contributions from the Lyα clouds and the diffuse intergalactic medium (IGM), this observation suggests that the spectrum of the UVB must be sufficiently soft. Since it is difficult to produce such a soft spectrum based on QSO origin, we need other sources of UVB which have a substantial UV emissivity and a softer spectrum than that of QSOs.

* Present address: Department of Physics, Tokyo Metropolitan University, 1-1 Minami-Ohsawa, Hachioji, Tokyo 192-03.

Here, we consider collapsing objects which liberate their gravitational energy by emitting photons. What is particularly important in this work is the inclusion of emission corresponding to the collisional excitation cooling of He II, which has been neglected in previous studies. The advantage of including this emission comes from the energy of the radiated photon; since the photon can ionize H I, but not He II, a soft spectrum of the resulting UVB is expected.

In section 2, the methods used to calculate the UVB flux and the UV source models are presented in detail. The results are described in section 3. Our discussion and conclusions are summarized in section 4.

2. UV Background and UV Source Models

2.1. The UVB Flux

The UVB flux $J(\nu, z)$ (erg s^{-1} cm^{-2} Hz^{-1} sr^{-1}) at frequney ν, as seen by an observer having a redshift of z, is given by

$$J(\nu, z) = \frac{1}{4\pi} \int_z^\infty \left(\frac{1+z}{1+z'}\right)^3 \varepsilon_{\rm tot}(\nu', z') \frac{dl}{dz'} dz', \qquad (1)$$

where $\varepsilon_{\rm tot}(\nu, z)$ is the proper volume emissivity, and

$$\nu' = \frac{1+z}{1+z'}\nu. \qquad (2)$$

For $\varepsilon_{\rm tot}(\nu, z)$ we consider two kinds of sources: the emissivity of collapsing objects $\varepsilon_{\rm c}(\nu, z)$ and that of QSOs

$\varepsilon_{\rm QSO}(\nu, z)$. For a Friedman universe with a density parameter Ω_0 and a Hubble constant H_0, the relation between the proper-length increment dl and the redshift increment dz is given by

$$\frac{dl}{dz} = \frac{c}{H_0}(1+z)^{-2}\,(1+\Omega_0 z)^{-1/2}\,, \tag{3}$$

where c is the velocity of light. We consider cold dark-matter (CDM) universes with $\Omega_0 = 1.0$ and 0.2. Throughout this paper we assume $h \equiv H_0/(100\ {\rm km\ s^{-1}\ Mpc^{-1}})$ is 0.5.

In equation (1), we neglect the absorption due to Lyα clouds, since we do not have complete information about the evolution of the Lyα clouds over the entire redshift range in which we are interested, $z = 0$–30. We briefly discuss this assumption below (section 4).

2.2. *Emissivity from Collapsing Objects*

In the CDM scenario, objects in the universe are formed through hierarchical clustering: smaller systems are formed earlier, and larger systems are formed later. In order to calculate the emissivity of collapsing objects, we need the formation rate $R_{\rm f}(z, M)dzdM$, at which objects with mass in the range M to $M+dM$ are formed in the redshift interval z to $z+dz$. Adopting the formalism developed by Kitayama and Suto (1996), the formation rate is given by

$$R_{\rm f}(z,M)dzdM = -\sqrt{\frac{2}{\pi}}\frac{1}{\sqrt{\sigma^2(M_{\rm f})-\sigma^2(M)}}\frac{d}{dz} \times \left[\frac{\delta_{\rm c}}{D(z)}\right] N_{\rm PS}(z,M)dzdM, \tag{4}$$

where $N_{\rm PS}(M, z)$ is the Press-Schechter mass function, $\delta_{\rm c}$ is equal to 1.69 for a flat universe and 1.64 for an open universe with $\Omega_0 = 0.2$ (Lilje 1992), $M_{\rm f} = M/2$, $D(z)$ is the linear growth factor, and $\sigma(M)$ is the root mean square of the density fluctuation smoothed over a region of mass M, for which we used the fitting formula of White and Frenk (1991). The biasing parameters which we used are 1.0 for $\Omega_0 = 1$ and 6.6 for $\Omega_0 = 0.2$, which are in accord with the two-year COBE-DMR normalizations (Gorski et al. 1995).

We assume that a forming object once virializes, and, subsequently, the baryonic component of the object contracts, dissipating its gravitational energy by radiative cooling. The density $\rho_{\rm vir}$, temperature $T_{\rm vir}$, and radius $R_{\rm vir}$ of virialized systems are calculated based on the spherical model. These quantities are summarized in the Appendix. Let f_R be the ratio of the final radius of the baryonic component to $R_{\rm vir}$. What is the appropriate value for f_R? Consider a typical spiral galaxy with mass $10^{12} M_\odot$ formed at $z = 2$, in the case of $\Omega_0 = 1.0$. The virial radius $R_{\rm vir}$ for this galaxy becomes 90 kpc$(h/0.5)^{-2/3}$ [equation (A2)]. Since the scale heights of the exponential disk of the spirals are typically several kiloparsecs (e.g., Mihalas, Binney 1981), the typical value of f_R would be around 0.1. In order to proceed analytically, we assume f_R to be constant throughout the calculation, and consider the cases of $f_R = 1$, 0.1, and 0.05.

Assuming that the gravitational potential in virialized objects is dominated by the contribution from dark matter, the total gravitational energy liberated in the redshift range of z to $(z+dz)$ by objects whose masses are in the range M to $(M+dM)$ is given by

$$\frac{d^2E}{dzdM}dzdM = \Omega_{\rm b} G M^2 \left(\frac{1}{f_R R_{\rm vir}} - \frac{1}{R_{\rm m}}\right) \times R_f(z,M)dzdM, \tag{5}$$

where the maximum radius $R_{\rm m}$ is taken to be $2R_{\rm vir}$, and we use the baryonic density parameter $\Omega_{\rm b} = 0.05$, which is consistent with big-bang nucleosynthesis.

The gas in collapsing objects is assumed to be in collisional equilibrium. Figure 1a shows the total cooling rate, $\Lambda_{\rm tot}$ [we assume the primordial mass fraction of helium, $Y = 0.245$, throughout this paper, and the cooling rates are taken from Cen (1992), and Fukugita, Kawasaki (1994)]. From this figure it is clear that $\Lambda_{\rm tot}$ is mostly determined by the bremsstrahlung and collisional excitation coolings of H I and He II. In the following we neglect the emission of collisional excitation cooling of H I because it is not relevant to the ionization of the IGM. We thus consider only the contributions of the bremsstrahlung and collisional excitation of He II.

The emissivity of collapsing objects $\varepsilon_{\rm c}$ is the sum of the bremsstrahlung emissivity $\varepsilon_{\rm ff}$ and the collisional excitation emissivity $\varepsilon_{\rm He,(bb)}$. Assuming that the temperature in objects remains constant at $T_{\rm vir}$ during the collapse, the emissivity of the radiative process i [= He(bb) or (ff)] per unit frequency per unit time at frequency ν and redshift z is expressed as

$$\varepsilon_i(\nu,z) = c\left(\frac{dl}{dz}\right)^{-1}(1+z)^3 \times \int_{M(z)} S_i(T_{\rm vir},\nu) f_i \frac{d^2E}{dzdM}dM, \tag{6}$$

where f_i is the ratio of the cooling rate of process i to the total cooling rate $\Lambda_{\rm tot}$ and $M(z)$ is the mass range of the integration. The spectrum of process i is given by

$$S_i(T,\nu) = \begin{cases} \delta(\nu-\nu_{\rm c}) & \text{for } i = \text{He(bb)} \\ g(\nu)(h_{\rm p}/kT)\exp(-h_{\rm p}\nu/kT) & \text{for } i = \text{ff}, \end{cases} \tag{7}$$

where $h_{\rm p}$ is the Planck constant, k is the Boltzmann constant, $h_{\rm p}\nu_{\rm c} = 40.8$ eV is the Lyα energy of He II, and $g(\nu)$ is the Gaunt factor normalized so that the integration of $S_{\rm ff}$ over the frequency is unity. We use the formulae of Rybicki and Lightman (1979) for the Gaunt factor.

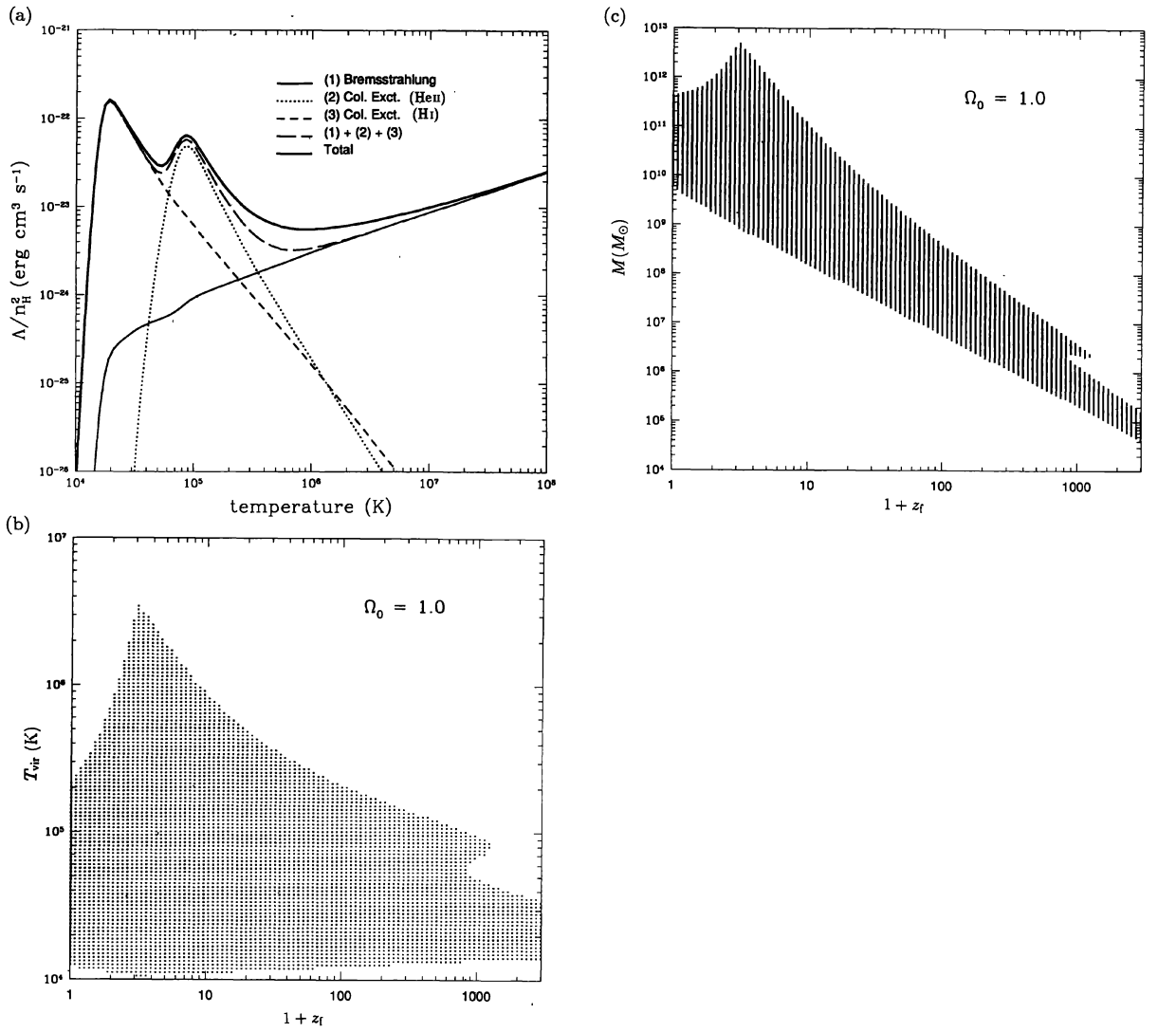

Fig. 1. Cooling condition for collapsing objects for a flat universe. (a) The cooling curve for the primordial gas. The contribution from dominant cooling processes to the total cooling rate (thick solid line) are shown as the thin solid line (bremsstrahlung), the dotted line (collisional excitation of He II), and the dashed line (collisional excitation of H I). (b) The virialized objects which have $T_{\rm vir}$ and the formation epoch $z_{\rm f}$ in the dotted region satisfy the cooling condition $t_{\rm rad} < \min(t_{\rm Comp}, t_0)$. (c) The same as (b), but $T_{\rm vir}$ is converted to the corresponding mass.

The mass range of integration $M(z)$ [equation (6)] is determined by comparing three time scales. If an object collapses at a high redshift, where the Compton cooling is efficient to cool objects, the gravitational energy of the object goes to the cosmic microwave background (CMB) and does not contribute to UVB. Also, if the radiative cooling time-scale of an object is longer than the age of the universe at the present epoch t_0, the collapsing object does not cool. Thus, an object serves as a UV source only when the time scale of the radiative cooling is shorter than both the time scale of the Compton cooling and the age of the universe. The time scale of the Compton cooling $t_{\rm Comp}$ is given by (Cen 1992)

$$t_{\rm Comp} = \frac{3}{8}\frac{m_{\rm e}c}{\sigma_{\rm T}}\frac{n_{\rm tot}}{n_{\rm e}}(1 - T_{\rm r}/T)^{-1}\,\epsilon_{\rm r}^{-1}, \qquad (8)$$

where $m_{\rm e}$ is the electron mass, $\sigma_{\rm T}$ the Thomson cross section, $n_{\rm e}$ the electron density, $n_{\rm tot}$ the total number density of the baryonic matter, $T_{\rm r}$ the temperature of the cosmic microwave background, and $\epsilon_{\rm r}$ the energy density of CMB. The time scale of the radiative cooling is given

Table 1. Adopted parameters for QSOs.

Ω_0	α	β_1	β_2	z_*	σ_*	$\log(L_*/L_\odot)$	$\log(\Phi_*/\mathrm{Gpc}^{-3})$
1.0	0.5	1.64	3.52	2.75	0.93	13.03	2.95
0.2	1.0	1.83	3.70	2.77	0.91	13.42	2.37

Table 2. Models considered and their names.

	$\Omega_0 = 1.0$	$\Omega_0 = 0.2$
QSO	FQ	OQ
QSO+($f_R = 0.05$)	FQS	OQS
QSO+($f_R = 0.1$)	FQM	OQM
QSO+($f_R = 1.0$)	FQL	OQL

by

$$t_{\rm rad} = \frac{3kTm_{\rm p}}{2\mu\Lambda_{\rm tot}X^2\rho_{\rm gas}}. \quad (9)$$

In the above, $X = 1 - Y$, $m_{\rm p}$ is the proton mass, $\rho_{\rm gas}$ the gas density, and μ the mean molecular weight for which we take the value for the fully ionized primordial gas. In figure 1b, the region which satisfies the condition $t_{\rm rad} < \min(t_{\rm Comp}, t_0)$ is shown as the dotted region on the $T_{\rm vir}$–z plane; the corresponding region on the M–z plane is shown in figure 1c. The upper-left and bottom boundary of the region correspond to the condition $t_{\rm rad} = t_{\rm Comp}$, and the upper-right boundary corresponds to $t_{\rm rad} = t_0$.

2.3. *Emissivity from QSOs*

The luminosity function and the evolutionary model for quasars are taken from Pei (1995). Based on the observational data of about 1200 quasars over the range of redshifts $0 \lesssim z \lesssim 4.5$, the fitted luminosity function $\phi(L, z)$ is expressed as

$$\phi(L,z) = \frac{\Phi_*}{L_z}\left\{\left(\frac{L}{L_z}\right)^{\beta_1} + \left(\frac{L}{L_z}\right)^{\beta_2}\right\}^{-1}. \quad (10)$$

In the above equation, the evolutionary model is characterized by the function L_z, which has a Gaussian form,

$$L_z = L_*(1+z)^{-(1-\alpha)}\exp[-(z-z_*)^2/(2\sigma_*)]. \quad (11)$$

We use the parameters derived by Pei (1995) (table 1). The QSO spectra in the UV range have a large observational uncertainty. We use the spectrum which is the same as the "medium" model of Meiksin and Madau (1993), and has the form:

$$F_\nu \propto \begin{cases} \nu^{-0.7} & \text{for } h_{\rm p}\nu < 10.2 \text{ eV}, \\ \nu^{-\alpha_{\rm Q,UV}} & \text{for } h_{\rm p}\nu > 10.2 \text{ eV}, \end{cases} \quad (12)$$

where $\alpha_{\rm Q,UV}$ is fixed to 1.5 throughout the calculation.

Finally, the emissivity of all quasars is calculated as

$$\varepsilon_{\rm QSO}(\nu, z) = \int \phi(L,z)(1+z)^3 F_\nu dL. \quad (13)$$

The models which we consider are summarized in table 2.

3. Results

The evolution of $J(\nu_{\rm H}, z)$ and $J(\nu_{\rm He}, z)$ ($h_{\rm p}\nu_{\rm H} = 13.6$ eV and $h_{\rm p}\nu_{\rm He} = 54.4$ eV are the ionization threshold energies of H I and He II, respectively) are plotted in figure 2. The thin lines are the UVB fluxes of models FQ and OQ (QSO alone), and the thick lines are those of models FQS, FQM, FQL, OQS, OQM, and OQL (QSO and collapsing objects).

In a flat universe (figure 2a), UVB of models FQS, FQM, FQL are considerably larger than when only QSO is considered (model FQ). At high redshifts ($z \gtrsim 4$), UVB is dominated by the emission from collapsing objects. The UVB due to collapsing objects rises steeply at $z \sim 30$, and remains almost constant down to $z \sim 3$. If objects contract sufficiently ($f_R \lesssim 0.1$; models FQM and FQS), UVB from collapsing objects is comparable to that from QSOs, even at $z \sim 2$ when UVB due to QSO is maximum. Also, the intensity at $\nu_{\rm H}$ is consistent with the UV flux suggested by the proximity effect, which is indicated by the box in figure 2 [$J(\nu_{\rm H}) = 10^{-21\pm0.5}$(erg s^{-1} cm^{-2} Hz^{-1} sr^{-1}) for $z = 1.7$–3.8; Bajtlik et al. (1988)]. Since the reionization of IGM starts at $z \sim 30$, it can be seen from figure 1c that the objects of the mass in the range 10^7–10^{12} $M_\odot$ give a high contribution to UVB.

On the other hand, in an open universe (figure 2b), the UV flux from collapsing objects is negligible at $z \lesssim 9$. This is because of the low power in the small-scale spectrum of the density fluctuation in an open CDM universe. Thus, in this case, the prediction for UVB is almost the same as that considering QSO alone, and the spectrum of UVB is too hard to explain the detected He II absorption.

Figure 3 shows the spectrum of UVB at several redshifts in a flat universe for $f_R = 0.05$ (model FQS). At $z \gtrsim 3$, there exists a bump due to the emission of the collisional excitation of He II just below the line energy $h_{\rm p}\nu_{\rm c}$. Owing to this bump, the spectrum is far from the

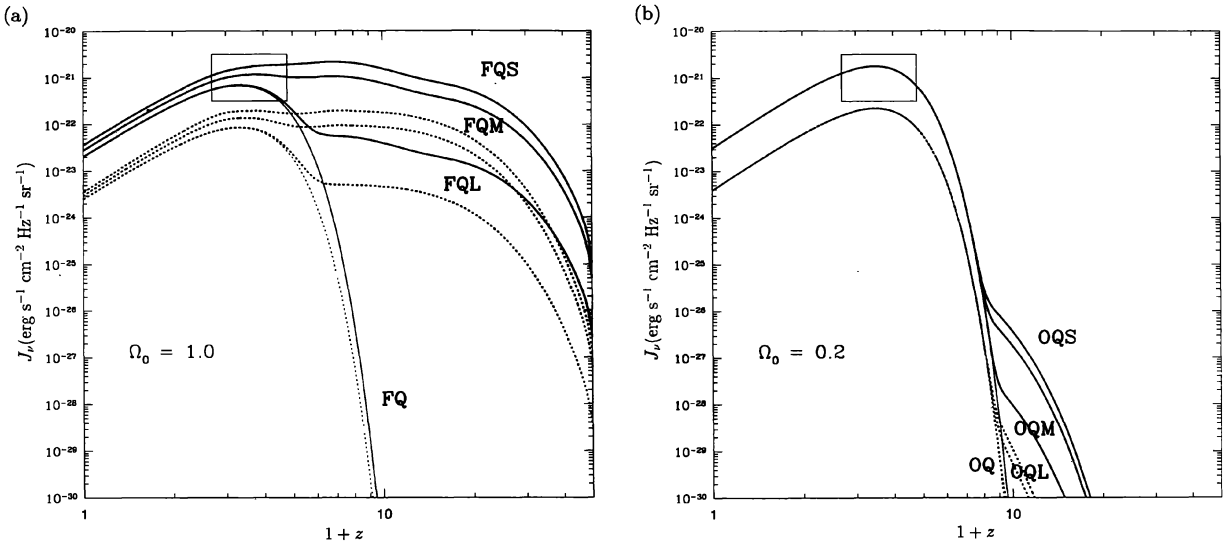

Fig. 2. Evolution of the UVB at $\nu = \nu_{\rm H}$ (solid line) and $\nu = \nu_{\rm He}$ (dotted line), for (a) $\Omega_0 = 1.0$ and for (b) $\Omega_0 = 0.2$. The contraction ratio f_R for three lines are 0.05, 0.1, and 1.0 from upper to lower, and the lowest line corresponds to the case in which QSO alone is concerned. The boxes indicate the flux required by observing the proximity effect.

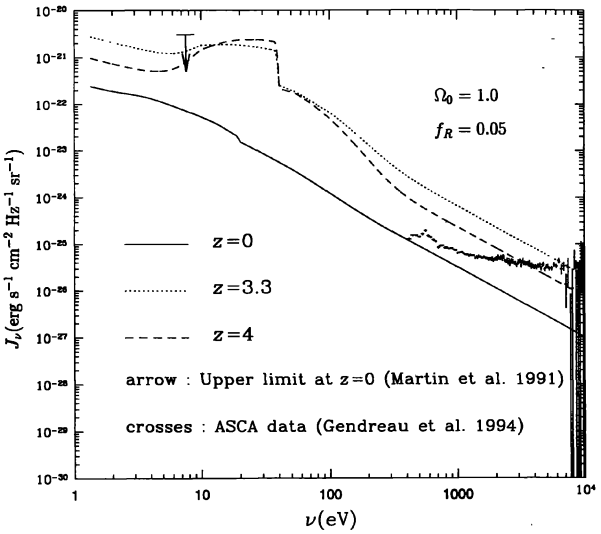

Fig. 3. Spectrum of UVB at several redshifts for $\Omega_0 = 1.0$ and $f_R = 0.05$. There exists a bump due to the collisional excitation emissivity of He II at $z = 4.0$ and 3.3 and higher redshifts. The arrow denotes the upper limit of UVB at the present epoch, and the crosses indicate the ASCA observations.

power law and becomes softer than in the case only with QSOs (see section 4). At $h_{\rm p}\nu \gtrsim 300$ eV, the UVB spectrum is well fitted by a power-law. On the other hand, at $h_{\rm p}\nu \lesssim 300$ eV, the UVB flux is larger than the value of extrapolation from higher frequencies. This component comes from the free-free emission of collapsing objects. At $z \lesssim 2$, the spectrum is well fitted by a power law with a spectrum index of ~ 1.5, which is the spectrum index of QSOs. Thus, it is expected that the He II/H I ratio changes at $z \sim 2$. The arrow in the figure shows the upper limit of UVB at $z = 0$ (Martin et al. 1991), which is well above our result. Our results are also consistent with the X-ray background observation by ASCA, which is indicated by the crosses in figure 3 (Gendreau et al. 1994).

With the flux and the spectrum obtained above, the ionization state of the IGM under the influence of UVB can be calculated assuming that the IGM is in photoionization equilibrium, and, that the IGM temperature is determined by requiring that the radiative cooling [the free-free cooling, the collisional excitation cooling of He II, the Compton cooling, and other cooling mechanisms listed in Cen (1992)] equals the photoionization heating. The evolutions of the ionization fractions of H and He are shown in figure 4 (the fraction of the diffuse IGM in the total baryonic matter in the universe, $f_{\rm IGM}$, is fixed at 1.0). In each panel, the thin lines are the results of models FQ and OQ, and the thick lines are those of models FQS and OQS. In a flat universe, the reionization process in the case with collapsing objects proceeds much earlier than in model FQ due to the extra UV photons. Because of the soft spectrum, the reionization epoch of H, when H is almost fully ionized, is earlier than that of He, when the He III fraction becomes nealy unity.

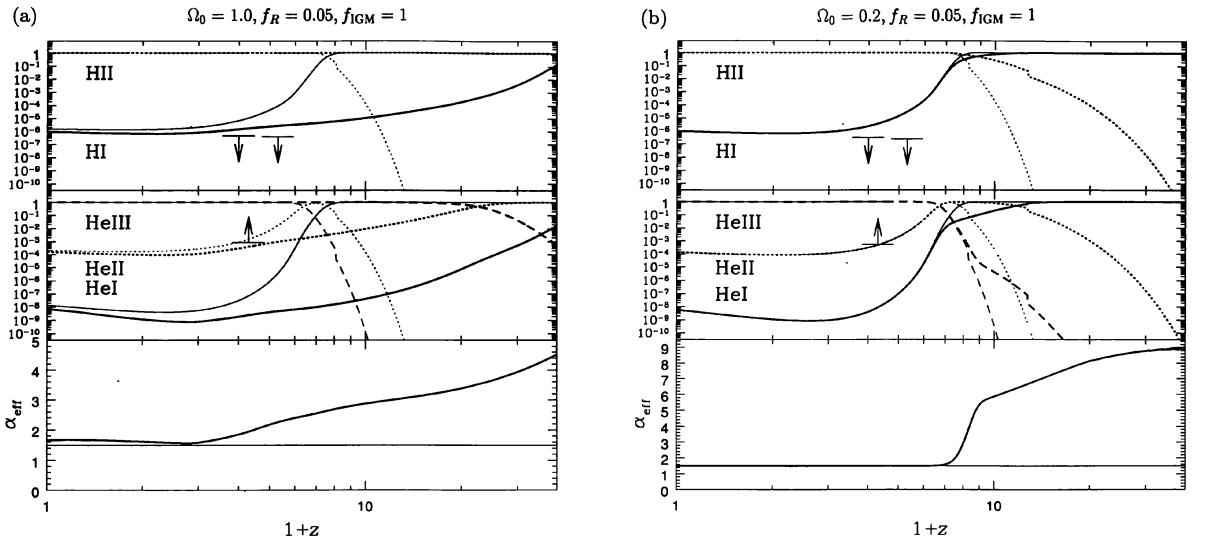

Fig. 4. Ionization fractions of IGM and the effective index [equation (18)] under photoionization equilibrium for (a) $\Omega_0 = 1.0$ and for (b) $\Omega_0 = 0.2$. The thick lines were calculated with the emission from both collapsing objects and QSOs, and thin lines were calculated with that from QSOs alone. In the top panel, the solid line and the dotted line are for $\tilde{\chi}_{HI}$ and for $\tilde{\chi}_{HII}$, respectively. In the middle panel, the solid line, the dotted line, and the dashed line represent $\tilde{\chi}_{HeI}$, $\tilde{\chi}_{HeII}$, and $\tilde{\chi}_{HeIII}$, respectively. The GP limits for $\tilde{\chi}_{HI}$ and $\tilde{\chi}_{HeII}$ are shown.

4. Discussion and Conclusions

The observations of the GP tests give the upper bound for the neutral fraction of H, χ_{HI}, in the diffuse component of IGM. We consider recent observations which give the 1σ upper limits: $\tau_{GP,HI} < 0.039$ at $z = 3.0$ and $\tau_{GP,HI} < 0.05$ at $z = 4.3$ (Giallongo et al. 1992; Giallongo et al. 1994). When IGM is almost fully ionized, the H I GP optical depth is given by

$$\tau_{GP,HI} = 1.0 \times 10^4 \left(\frac{h}{0.5}\right)^{-1} \times f_{IGM}^2 \tilde{\chi}_{HI}(1+z)^2(1+\Omega_0 z)^{-1/2}, \quad (14)$$

where $\tilde{\chi}_{HI}$ is the neutral fraction of H in the case of $f_{IGM} = 1$.

The upper bound on $\tilde{\chi}_{HI}$ is shown by the arrows in figure 4. The value of $\tilde{\chi}_{HI}$ at $z = 3.0$ of the FQS model is 1.42×10^{-6}, which is consistent with the observation if $f_{IGM} < 0.40$. At $z = 4.3$, $\tilde{\chi}_{HI} = 2.59 \times 10^{-6}$, which gives $f_{IGM} < 0.27$. In the model OQS, the upper limits for f_{IGM} were obtained as $f_{IGM} < 0.37$ at $z = 3.0$ and $f_{IGM} < 0.09$ at $z = 4.3$.

The recent observation of the quasar Q0302−003 at $z = 3.286$ gives a lower limit of the He II optical depth: $\tau_{HeII} > 1.7$ at $z \simeq 3.3$ (Jakobsen et al. 1994). Assuming that this absorption is completely due to the diffuse IGM, the He II GP optical depth is given by

$$\tau_{GP,HeII} = 2.2 \times 10^2 \left(\frac{h}{0.5}\right)^{-1} \times f_{IGM}^2 \tilde{\chi}_{HeII}(1+z)^2(1+\Omega_0 z)^{-1/2}. \quad (15)$$

The value of χ_{HeII} at $z = 3.3$ in our calculation is 4.07×10^{-4} in the FQS model. In this case $\tau_{GP,HeII}$ becomes 0.80, even with $f_{IGM} = 1$, which is lower than the observational constraint. Thus, provided that the reported He II absorption is completely due to the smoothly distributed IGM, observations of H I and He II GP tests cannot be satisfied simultaneously with our spectrum.

The constraint for the UVB spectrum can be relaxed, however, if the filtering of UVB by the intervening Lyα clouds is considered and the absorption reported is a consequence of the combination of the absorption in IGM and Lyα clouds (Giroux et al. 1995). In order to compare our results with the constraint in such a situation, we define the effective index α_{eff} as the index of the power-law spectrum, which can give rise to the ionization fractions of our results. If He I fraction in the IGM is sufficiently small, the ionization fractions depend on the UV spectrum through the photoionization rates of H I and He II,

$$\Gamma_{HI} = \int_{\nu_H}^{\infty} \frac{J(\nu)}{h_p \nu} \sigma_H(\nu) d\nu, \quad (16)$$

$$\Gamma_{HeII} = \int_{\nu_{He}}^{\infty} \frac{J(\nu)}{h_p \nu} \sigma_{HeII}(\nu) d\nu, \quad (17)$$

where the photoionization cross sections of H I and He II are denoted by σ_H and σ_{HeII}. Then, the effective index

is defined by

$$4 \times 4^{\alpha_{\rm eff}} \equiv \frac{\Gamma_{\rm H\,I}}{\Gamma_{\rm He\,II}}. \quad (18)$$

When the gas is in photoionization equilibrium and almost fully ionized, $\alpha_{\rm eff}$ is related to the following ionization fractions:

$$\frac{\chi_{\rm HeII}}{\chi_{\rm HI}} = \frac{\alpha_{\rm He\,III}}{\alpha_{\rm H\,II}} \frac{\Gamma_{\rm H\,I}}{\Gamma_{\rm He\,II}} = 22 \times 4^{\alpha_{\rm eff}}, \quad (19)$$

where $\alpha_{\rm H\,II}$ and $\alpha_{\rm He\,III}$ are the recombination rates of H II and He III, respectively. The evolution of $\alpha_{\rm eff}$ is also plotted in figure 4. It shows that including the line emission of He II results in an increase of $\alpha_{\rm eff}$ from $\alpha_{\rm Q,UV} = 1.5$ to 1.9 at $z = 3.3$. Although it remains to be investigated how intervening Lyα clouds affect UVB with the emission from collapsing objects, if we simply compare it with figure 5 of Giroux et al. (1995) this result is consistent with the observations.

It is noted that the inclusion of the absorption by the intervening Lyα clouds may reduce the UVB flux by a factor of 4–6 (Madau 1992). Then, the emission from only QSOs cannot produce sufficient UVB to explain the proximity effect. However, if there is a sufficient contribution from collapsing objects (model FQS), the UVB intensity becomes consistent with the proximity effect.

If the reionization of IGM occurs at sufficiently high redshifts, the CMB spectrum will be distorted by Compton scattering. The y-parameter calculated from models FQS and OQS are 4.8×10^{-6} and 4.2×10^{-7}, respectively. These values are below the current observational constraint from the COBE-FIRAS data, $|y| < 2.5 \times 10^{-5}$ (Mather et al. 1994). The value of the y-parameter of the FQS model may be observed by future satellite experiments.

In summary, we performed calculations of the UVB flux and spectrum, considering the emission from collapsing objects as well as QSOs. It is shown that collapsing objects can serve as a dominant energy source for UVB, especially at high redshifts. Although the resulting spectrum is not consistent with the GP tests of H I and He II if they are due to the smoothly distributed IGM, our model calculation becomes consistent with observations if modifications are taken into account, such as absorption in the intervening absorption systems and the combined He II absorption of IGM and Lyα clouds.

We are grateful to Tatsushi Suginohara for useful discussions, and to Tetsu Kitayama who kindly gave us his code for computing the formation rate of objects. This research was supported in part by a Grant-in-Aid by the Ministry of Education, Science, Sports and Culture of Japan (No. 4294).

Appendix.

In a flat universe, the mean density of a virialized object is calculated on the basis of the spherical model (Peebles 1980; Suto 1993):

$$\rho_{\rm vir} = 18\pi^2(1+z)^3\rho_{\rm c} = 3.33 \times 10^{-27}(1+z)^3 h^2 \ {\rm g\ cm^{-3}}, \quad (A1)$$

where $\rho_{\rm c}$ is the critical density. Thus, the radius, temperature, and electron density of a virialized object with mass M are

$$R_{\rm vir} = \left(\frac{3M}{4\pi\rho_{\rm vir}}\right)^{1/3} = 5.23 \times 10^{19} \left(\frac{M}{M_\odot}\right)^{1/3} (1+z)^{-1} h^{-2/3} \ {\rm cm}, \quad (A2)$$

$$T_{\rm vir} = \frac{G m_{\rm p} M \mu}{3 k R_{\rm vir}} = 1.02 \times 10^{-2} \mu \left(\frac{M}{M_\odot}\right)^{2/3} (1+z) h^{2/3} \ {\rm K}, \quad (A3)$$

$$n_{\rm e,vir} = \frac{\Omega_{\rm b}\rho_{\rm vir}}{m_{\rm p}} \left(X + \frac{Y}{2}\right) = 1.99 \times 10^{-3}(1+z)^3 \left(X + \frac{Y}{2}\right) \Omega_{\rm b} h^2 \ {\rm cm^{-3}}. \quad (A4)$$

In an open universes, the radius of the virialized object is given by

$$R_{\rm vir} = \frac{(GM)^{1/3}}{1-\Omega_0} \left[\frac{\Omega_0(\sinh\theta_f - \theta_f)}{4\pi H_0}\right]^{2/3}, \quad (A5)$$

$$\theta_f = {\rm arccosh}\left[1 + \frac{2(1-\Omega_0)}{\Omega_0(1+z_f)}\right]. \quad (A6)$$

References

Bajtlik S., Duncan R.C., Ostriker J.P. 1988, ApJ 327, 570
Bechtold J., Weymann R.J., Lin Z., Malkan M.A. 1987, ApJ 315, 180
Cen R. 1992, ApJS 78, 341
Fukugita M., Kawasaki M. 1994, MNRAS 269, 563
Gendreau K.C., Mushotzky R., Fabian A.C., Kii T., Holt S.S., Serlemitsos P.J., Tanaka Y., Ogasaka Y. et al. 1994, in New Horizon of X-Ray Astronomy — first results from ASCA, ed F. Makino, T. Ohashi (Universal Academy Press, Tokyo) p365
Giallongo E., Cristiani S., Trevese D. 1992, ApJL 398, L9
Giallongo E., D'Odorico S., Fontana A., McMahon R.G., Savaglio S., Cristiani S., Molaro P., Trevese D. 1994, ApJL 425, L1
Giroux M.L., Fardal M.A., Shull J.M. 1995, ApJ 451, 477

Gorski K.M., Ratra B., Sugiyama N., Banday A.J. 1995, ApJL 444, L65
Gunn J.E., Peterson B.A. 1965, ApJ 142, 1633
Jakobsen P., Boksenberg A., Deharveng J.M., Greenfield P., Jedrzejewski R., Paresce F. 1994, Nature 370, 35
Jenkins E.B., Ostriker J.P. 1991, ApJ 376, 33
Kitayama T., Suto Y. 1996, MNRAS 280, 638
Lilje P.B. 1992, ApJL 386, L33
Madau P. 1992, ApJL 389, L1
Martin C., Hurwitz M., Bower S. 1991, ApJ 379, 549
Mather J.C., Cheng E.S., Cottingham D.A., Eplee R.E. Jr, Fixsen D.J., Hewagama T., Isaacman R.B., Jensen K.A. 1994, ApJ 420, 439
Meiksin A., Madau P. 1993, ApJ 412, 34
Mihalas D., Binney J. 1981, Galactic Astronomy, 2nd ed (W.H.Freeman and Company, New York) p326
Miralda-Escudé J., Ostriker J.P. 1990, ApJ 350, 1
Overduin J.M., Wesson P.S., Bowyer S. 1993, ApJ 404, 460
Pei Y.C. 1995, ApJ 438, 623
Peebles P.J.E. 1980, The Large-Scale Structure of the Universe (Princeton University Press, New Jersey) p77
Rybicki G.B., Lightman A.P. 1979, Radiative Processes in Astrophysics (John Wiley and Sons, New York) p160
Sasaki S., Takahara F. 1994, Prog. Theor. Phys. 91, 699
Sasaki S., Takahara F., Suto Y. 1993 Prog. Theor. Phys. 90, 85
Shapiro P.R., Giroux M.L. 1987, ApJL 321, L107
Suto Y. 1993, Prog. Theor. Phys. 90, 1173
White S.D.M., Frenk C.S. 1991, ApJ 379, 52